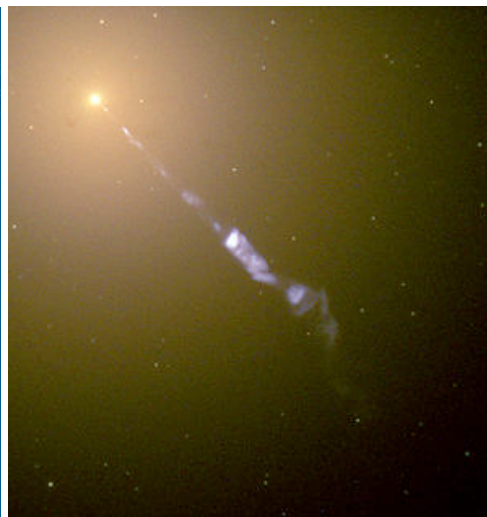
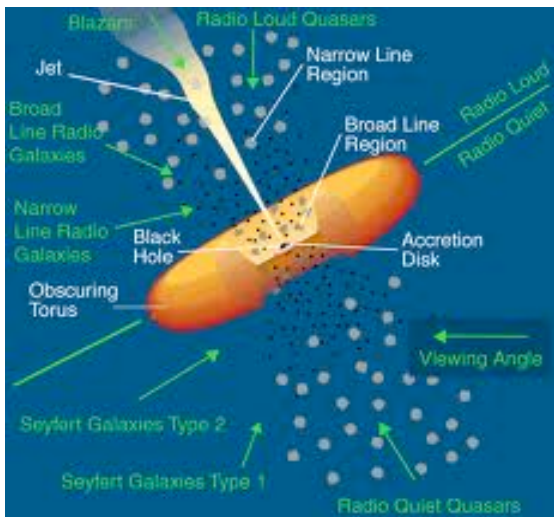
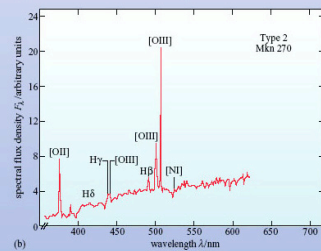
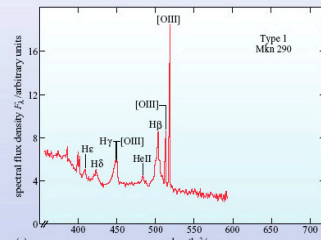


Active Galactic Nuclei

An Introduction to the Taxonomy, Spectra, Morphology and Evolution of the Most Energetic Objects in the Universe



Philip Hall
November 2011

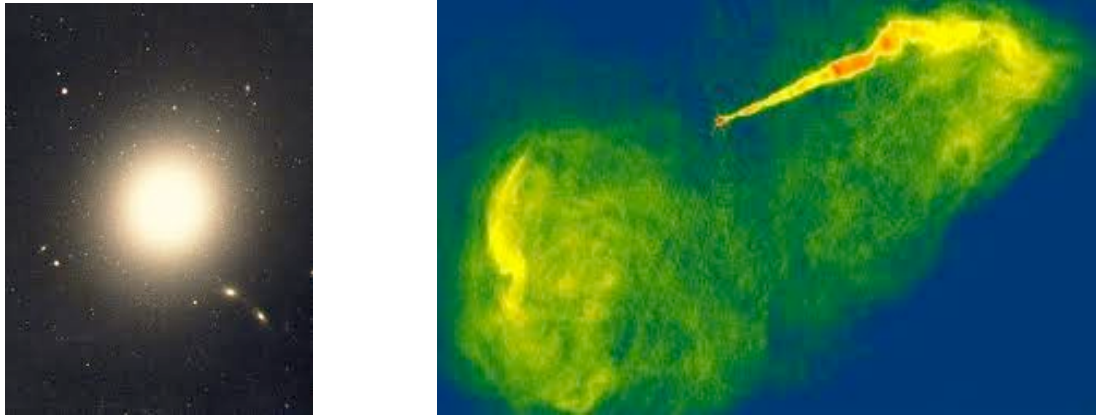
1. Introduction: The Concept of Active Galaxies

Active galaxies are galaxies exhibiting unusually energetic events in their nuclei that cannot be attributed directly to stars (Petersen, 1997) or to emission from gas heated by them (Sparke & Gallagher, 2007). The energy arises in a central region that is extremely small compared to the galaxy as a whole, hence the term *active galactic nuclei* (AGN) is employed to describe these objects. An active galaxy can be regarded as a normal galaxy that also contains an AGN (Jones & Lambourne, 2003).

Active galaxies are often difficult to distinguish from conventional galaxies in optical images (Figure 1, Left), but are clearly differentiated by their *spectra*, which exhibit unusual features from radio through to γ -ray wavelengths. In particular, the spectra show evidence of ionized gas in the nuclei not due to OB stars (Osterbrock & Ferland, 2006). Other characteristics include Doppler broadened emission lines^[1] and luminosity variable over short timescales. Some AGN have powerful radio jets emanating from the nucleus (Falcke, 2008) (Figure 1, Right).

Figure 1 (Left): The Active Galaxy M87 in Visible Light

Figure 1 (Right): M87 Central Region at Radio Wavelengths with Energetic Jet



Source: National Optical Astronomy Observatory and National Radio Astronomy Observatory

This paper reviews the history of active galaxy discovery (Section 2) and examines the taxonomy (Section 3) and spectral features (Section 4) of the four main types of active galaxy: *Seyferts*, *quasars*, *radio galaxies* and *blazars*.

All AGN share the property of prodigious energy output (10^{40} - 10^{47} erg s^{-1} or $2 \times 10^6 \sim 10^{13} L_{\odot}$) from a region little larger than the Solar System (Migliori, 2010). The proposed mechanism, gravitational in-fall onto a central *supermassive black hole* (SMBH) via an accretion disc, is now convincing (Peterson, 2004) and is reviewed in Section 5. The accretion disc radiates intensely in the UV to X-ray bands and is responsible for the luminosity of the AGN. It is surrounded by *broad and narrow spectral line regions* (BLRs and NLRs) of high and low velocity gas, but is obscured at certain viewing angles by a dusty torus (Urry & Padovani, 1995). The *AGN unified model*, which proposes that the AGN sub-types constitute the same underlying phenomenon under different viewing angles, is reviewed in Section 6, along with a potential evolutionary sequence for AGN in Section 7. The major outstanding problems in AGN research are briefly assessed in Section 8.

[1] The light from an astronomical object is the sum of individual photons emitted by atoms in motion, some approaching and some receding from the observer. The *velocity dispersion* (range of speeds) along the line of sight (Δv) produces *Doppler broadening* and is given by $\Delta\lambda/\lambda \approx \Delta v/c$, where λ is the central wavelength of the spectral line and c is the speed of light.

The motion of the atoms is due to their temperature, and the velocity dispersion for a gas of mass m and temperature T is given by:

$$\Delta v \approx \sqrt{\frac{kT}{m}} \text{ where } k \text{ is the Boltzmann constant } (1.38 \times 10^{-23} \text{ JK}^{-1}) \text{ (Jones \& Lambourne, 2003) (1.1)}$$

Active galaxies are rare. Even the most common type of AGN, the Seyfert galaxies, occurs at a rate of $10^{-4}/\text{Mpc}^3$ [2], or three orders of magnitude lower than the observed density of normal galaxies (Osterbrock & Ferland, 2006). Accordingly, the question of whether an AGN phase never occurs in most galaxies, or is a common, but short-lived feature of galactic evolution, is also addressed herein.

2. The History of Active Galaxy Discovery

2.1 Seyfert Galaxies

The first recorded observation of an AGN was of NGC 1068 (M77) by Edward Fath (1908) and subsequently confirmed by Slipher (1917). Both astronomers found an emission spectrum similar to gaseous nebulae, and Slipher reported a redshift implying a recessional velocity of 1100km s^{-1} . This was followed by the first visual confirmation of what turned out to be an AGN when Herber Curtis (1918) observed a “curious straight ray apparently connected with the nucleus [of M87] by a thin line of matter”.

The next major advance was Carl Seyfert’s (1943) discovery that several more galaxies in addition to NGC 1068 featured bright, point-like nuclei and broad emission lines (Figure 2, Left). As the first astronomer to identify them as a distinct group, this AGN sub-type now bears his name. In addition to their optical peculiarities, radio emissions from two Seyfert galaxies, NGC 1068 and NGC 1275, were detected in 1955 (Camenzind, 2002). Byrd et al. (1987) found that 73% of Seyferts have a companion galaxy, which suggests tidal interactions play an important role in their activity (Figure 2, Right),

Figure 2 (Left): Seyfert Galaxy NGC 4051 (distance 9.7 Mpc)

False colours are used to denote surface brightness (SB). Blue and green indicate low SB while yellow and red areas have high SB. The galaxy’s nucleus is tiny, but intensely luminous.

Figure 2 (Right): Seyfert Galaxy NGC 1097/1097A (distance ~14.5Mpc)

Emission lines in NGC 1097’s core display shock-excited characteristics with strong shear, which may channel gas inward to fuel the SMBH (Prieto et al. 2005). Note also companion galaxy NGC 1097A near the upper left corner.



Source: NASA/JPL and European Southern Observatory

2.2 Quasars

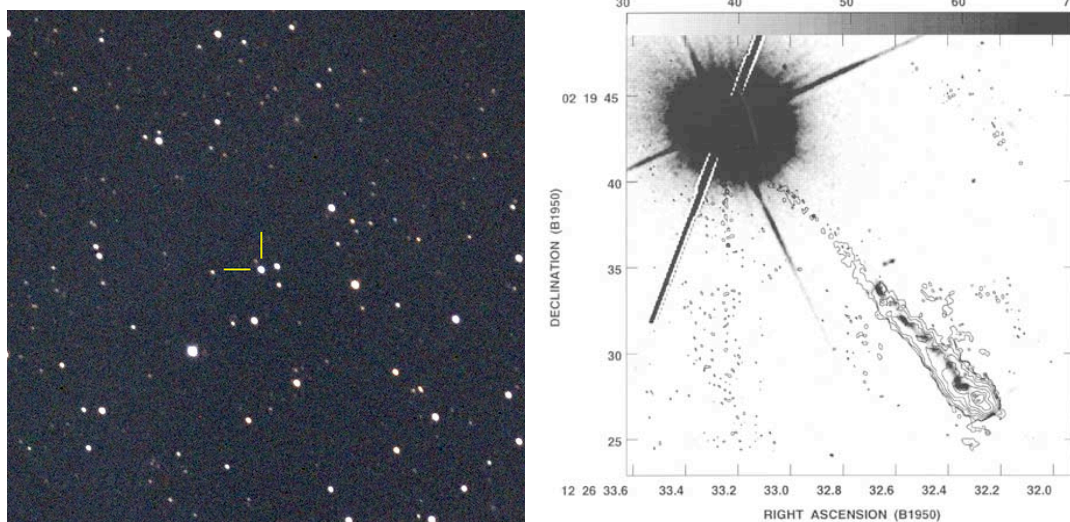
The next class of AGN, the quasars, was first detected in the 1950s when astronomers discovered a number of strong, unidentified radio sources. Radio astronomy was still in its infancy and resolution was initially too poor to pinpoint the location of the mysterious objects. However, Minkowski (1960) determined that one source, named 3C 295, was in the same position as a faint “star” whose redshift implied a cosmological distance and suggested a luminous galaxy or galaxy cluster.

[2] Mpc is an abbreviation for megaparsec (3.26×10^6 light years or $3.09 \times 10^{22}\text{m}$)

Matthews and Sandage (1963) employed the new technique of *interferometry* (the use of two physically separated radio dishes to improve resolution, in this case to 10 arcseconds). They determined that two radio sources, 3C 48 and 3C 196, were located at the same position as a faint star-like object to within the margin of observational error. Their spectra were unlike those of normal stars and bore some resemblance to old novae, but the authors did not suggest that it what they were. Shortly afterwards, Greenstein and Matthews (1963) determined that 3C 48 had a large redshift ($z=0.3675$)^[3], suggesting the source was an external galaxy and must be intensely luminous. Emission lines were detected in the spectrum.

The precise location of another radio source, 3C 273, was pinpointed by Hazard et al. (1963) using a lunar occultation. A double source separated by 20 arcseconds and consisting of a faint star-like object and jet was confirmed (Figure 3). As with 3C 48, it was soon ascertained that 3C 273 had a high red shift and was associated with an optical counterpart (Schmidt, 1963). The class of objects came to be known as *quasi-stellar radio sources*, or quasars. Although radio observations were crucial in detecting the first quasars, it has subsequently been found that most (90%) are *radio quiet*. Only 10% of quasars belong to the *radio loud* sub-type. The differences are explored in more detail later in this paper.

Figure 3 (Left): The Star-Like Visual Appearance of Quasar 3C 273
Figure 3 (Right): HST Gray-Scale Image of 3C 273 with Radio Jet and Contours



Sources: Flickr.com and Tour of the Radio Universe website

2.3 Radio Galaxies

The post-World War II advances in radio astronomy that led to the discovery of quasars are also associated with another class of AGN, the radio galaxies. Grote Reber was an electrical engineer and amateur radio operator who constructed the world's first radio telescope in his backyard in Wheaton, Illinois, in 1937. Two years later, he identified a strong radio source in the constellation Cygnus (Schilling, 2011). Hey et al. (1946) confirmed short-term fluctuations in the intensity of radiation from the same region, which was shown by Bolton and Stanley (1948) to originate in a small, discrete source of less than 8 arcminutes diameter. The object was first imaged by Baade (1951, Figure 4, Left) using the Palomar 200 inch reflector and identified as a double radio source (Jennison & Das Gupta, 1953).

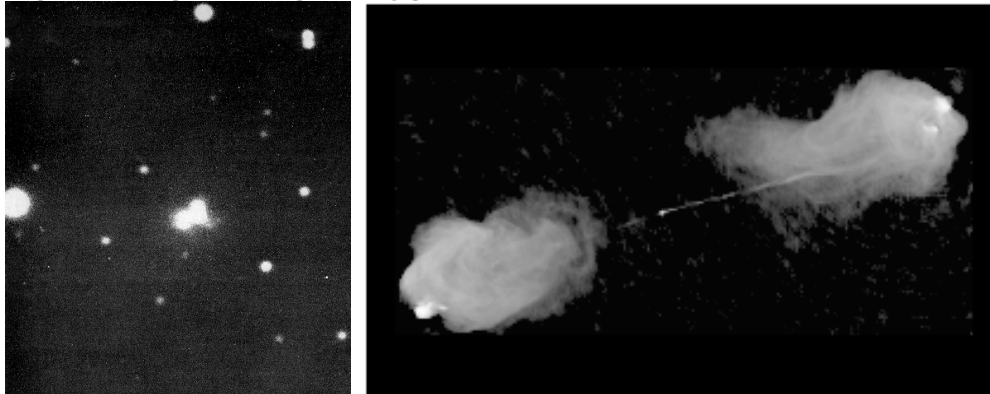
[3] The *redshift* (z) of an object is the relationship between the observed wavelength (λ) of a spectral line and the rest wavelength (λ_0) of the same line determined in the laboratory. It is given by:

$$z = \frac{\lambda}{\lambda_0} - 1 \quad (\text{Osterbrock \& Ferland, 2006}) \quad (2.2.1)$$

The double source was initially misinterpreted as two colliding galaxies (Baade & Minkowski, 1954), but gradually came to be accepted as a two-lobed structure emanating from a single source. High dynamic range images later settled the issue beyond doubt (Perley et al., 1984) (Figure 4, Right). Radio emissions from these galaxies are not of thermal origin. Rather, they are *synchrotron radiation* produced by charged particles moving in magnetic fields at relativistic speeds.

Figure 4 (Left): Walter Baade's 1951 Photograph of Cygnus A

Figure 4 (Right): Image of Cygnus A at 5 GHz with Resolution 0.4 Arcseconds



Source: Steinicke, Cygnus A website and Perley et al. 1984

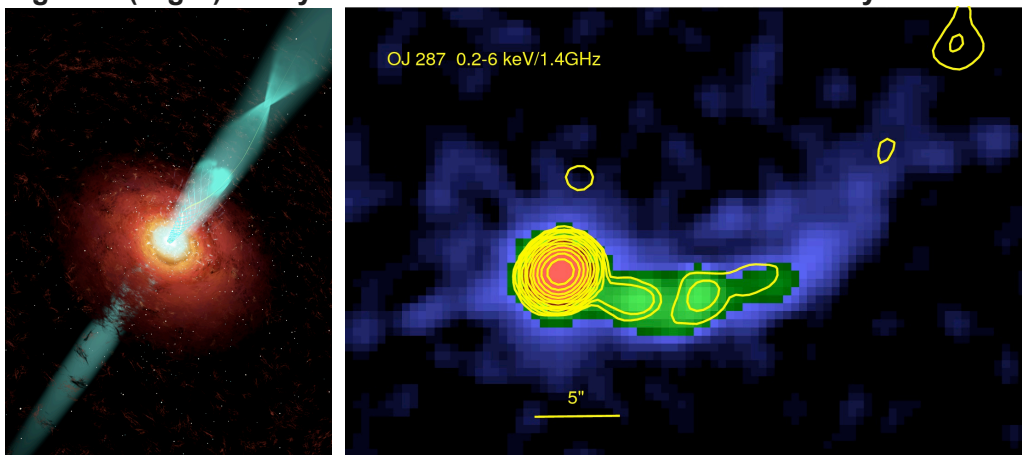
2.4 Blazars

Blazars, the most recently identified category of AGN, were originally thought to be irregular variable stars due to their rapid and unpredictable brightness variations and star-like visual appearance. The prototype blazar, BL Lacertae, was discovered and presumed to be variable star by Hoffmeister (1929). It varies between a visual magnitude of 13.0 and 16.1 over a few days (Semakin, 1955). It was first identified as a radio source by Schmitt (1968), but exhibited no emission or absorption lines (Oke et al. 1969), which argued strongly against a stellar explanation. Distance measurements later established it to be an external galaxy (Oke & Gunn, 1974).

The true nature of BL Lacertae was not a major surprise given the 1969 spectral findings. Strittmatter (1972) had already proposed a new AGN class, the BL Lacs, to classify objects with the observed properties of rapid variability (at optical, infrared or radio wavelengths), the absence of emission lines, and strong and rapidly varying polarization. These characteristics are thought to be a consequence of the AGN jet being aligned directly towards the Earth (Figure 5; see also Section 6). The BL Lacs are now recognized as one blazar sub-type, the other being Optically Violent Variables (OVVs). Within the blazar class, OVVs have greater luminosity and inferred *Lorentz factors* (see Section 6.5 for explanation) than the BL Lacs (Peterson & Wilkes, 2006).

Figure 5 (Left): Blazar Jet

Figure 5 (Right) X-Ray Contours of Blazar OJ287 Point Directly to Earth



Source: Boston University Blazar Research; Chandra X-Ray Observatory

3. Active Galaxies: Major Taxonomy and Sub-Types

The classification of AGN is based around the four major types previously described, and this section presents the criteria used to allocate a galaxy to a particular class. The taxonomy of AGN is set out in Table 1 and incorporates the schemes of Blandford et al. (1990), Urry & Padovani (1995) and Peterson (1997).

The major considerations in classification are radio emission (strong [S] or weak [W]) and the broad and narrow emission lines, which may be absent, weak or strong. In some cases, both weak and strong examples have been observed and are denoted [SW] in Table 1. Most AGN classes are specifically associated with either large spiral (S) or elliptical (E) galaxies. No AGN are known in dwarf or irregular galaxies.

Each of the four main AGN classes has two recognized sub-types, also set out in Table 1. For example, Seyferts are split between Type 1 (Sy1), where broad emission lines are evident, and Type 2 (Sy2), where they are absent. However, the real universe resists these simple divisions, and Osterbrock (1977) introduced sub-types 1.2, 1.5, 1.8 and 1.9 for Seyferts with progressively weakening broad lines.

Table 1: Broad Classification Scheme for AGN

		Galaxy Type	Radio Emission	Emission Lines	
				Broad	Narrow
Seyferts	Seyfert 1	Sa-Sbc	W	SW	SW
	Seyfert 2	Sa-Sbc	W	None	SW
Quasars	Radio-Quiet Quasar	S/E	W	S	SW
	Radio-Loud Quasar	E	S	S	SW
Radio Galaxies	Narrow Line Radio Galaxy	E	S	W	S
	Broad Line Radio Galaxy	E	S	S	W
Blazars	BL Lacertae (BL Lacs)	E	S	None	None/W
	Optically Violent Variables	E	S	S	W

Emission/Radio Labels are: S=Strong; W=Weak; SW: Strong & Weak examples observed

Sources: Blandford et al. (1990); Urry & Padovani (1995); Peterson (1997)

Radio loud AGN are strongly associated with elliptical galaxies while radio quiet AGN occur in spirals, but the reasons why some AGN are radio loud and others quiet are not well understood. Radio emission appears to be only weakly dependent on SMBH mass (Woo & Urry, 2002), but more strongly on SMBH spin and accretion disc temperature (Whittle, 2011). In order to generate a sufficient magnetic field to collimate the radio jets, charged particles in orbit around the SBMH must be in rapid motion, drawing their energy from the SMBH's rotation (Peterson & Wilkes, 2006). Accordingly, it may be that radio jets occur only in AGN with rapidly spinning black holes.

Distinctions between certain AGN sub-types can be subtle. Radio quiet quasars display striking similarities to the Sy1 sub-class, and the difference may reduce to the greater *bolometric luminosity* (integrated luminosity across all electromagnetic wavelengths) of the quasars. This is a function of the mass and mass accretion rate of the SMBH (see Section 5). In quasars, the most powerful type of AGN, the luminosity of the nucleus (L_{nuc}) exceeds the entire host galaxy (L_{gal}), whereas in moderate AGN $L_{nuc} \leq L_{gal}$, and in weak AGN $L_{nuc} \ll L_{gal}$ (Whittle, 2011). Radio-loud quasars and the broad line radio galaxies also have comparable spectra. The similarities across classes suggest the various AGN have much in common, a theme to which we return in Section 6.

AGN morphology has been pieced together over decades by many different researchers and inevitably a variety of technical terms have come into use, some of which overlap. Among the blazars, the optically violent variables (OVVs) are also sometimes known as *flat-spectrum radio quasars* (FSRQs). Less luminous AGN (10^{38} - 10^{40} erg s⁻¹) may be referred to as LINERs (Low Ionization Nuclear Emission-line Regions). As the name implies, LINERs exhibit softer ionization, with markedly weaker [O III] emissions, but low ionization species such as [O I] and [N I] are relatively strong (Heckman, 1980). They are radio quiet and resemble Sy2 galaxies.

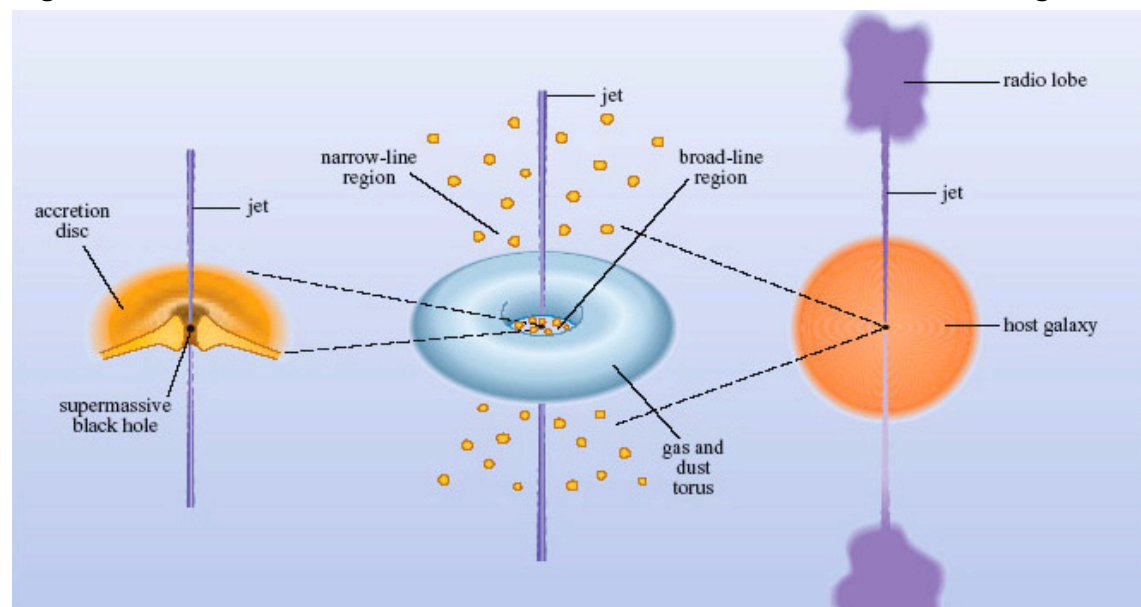
Certain additional refinements have also been introduced to cover the broad range of observed AGN phenomena. *Fanaroff and Riley Types I and II* (FR I and FR II) are terms used to describe the strength of collimated emission jets from the AGN. FR II jets are highly collimated and extend to bright hotspots (“edge-brightened”) far from the galaxy, while FR I jets are centrally bright but edge-darkened, and terminate closer to the galaxy’s centre. The labels are commonly appended to descriptions of radio galaxies and blazars.

4. The Spectra of Active Galaxies

We now proceed to examine the spectral characteristics of the various types of AGN. We noted earlier that spectral lines may be Doppler broadened due to the velocity dispersion of the emitting atoms in accordance with $\Delta\lambda/\lambda \approx \Delta v/c$. Doppler broadening is therefore to be expected when the emitting object is rotating, or gas is moving radially toward or away from the centre along the line of sight. The degree of broadening is commonly expressed as a speed, and is used to differentiate between the broad and narrow line emission spectra. Broad lines exhibit have speeds as high as $10\,000\text{km s}^{-1}$. In the context of AGN, narrow lines are generally defined by speeds of $<1000\text{km s}^{-1}$, although such speeds are still high by comparison with the spectra of more conventional objects such as stars and the Sun.

The detailed structure of AGN is covered in Section 6, but it is useful at this stage to be familiar with the general arrangement of the SMBH and accretion disc (Figure 6, Left). These are minutely sized, but extremely dense objects at the very centre of the active galaxy. Immediately outside lie the high-speed gas clouds responsible for the broad line spectra. They in turn are surrounded by a *torus* of dusty material. Beyond the torus lies the lower speed gas that generates the narrow line spectra (Figure 6, Centre). It is important to understand that the area represented in the central section of Figure 6 is itself extremely small relative to the active galaxy as a whole (Figure 6, Right).

Figure 6: General Structure of an AGN and the Broad and Narrow Line Regions



Source: Open University

AGN spectra display both *permitted* and *forbidden* lines. Radiative (but not collisional) transitions by electrons between bound states in an atom are governed by *selection rules*, especially as regards angular momentum. Transitions which follow these rules are known as *permitted transitions*, and have a high probability of occurrence. *Forbidden lines* are produced by transitions that do not obey the angular momentum rules and occur only rarely. If the upper state of a transition is unable to decay by a permitted transition, the atom is said to be *metastable*. In a high-density gas, de-excitation of metastable atoms is achieved through collisions, but in an extreme low-

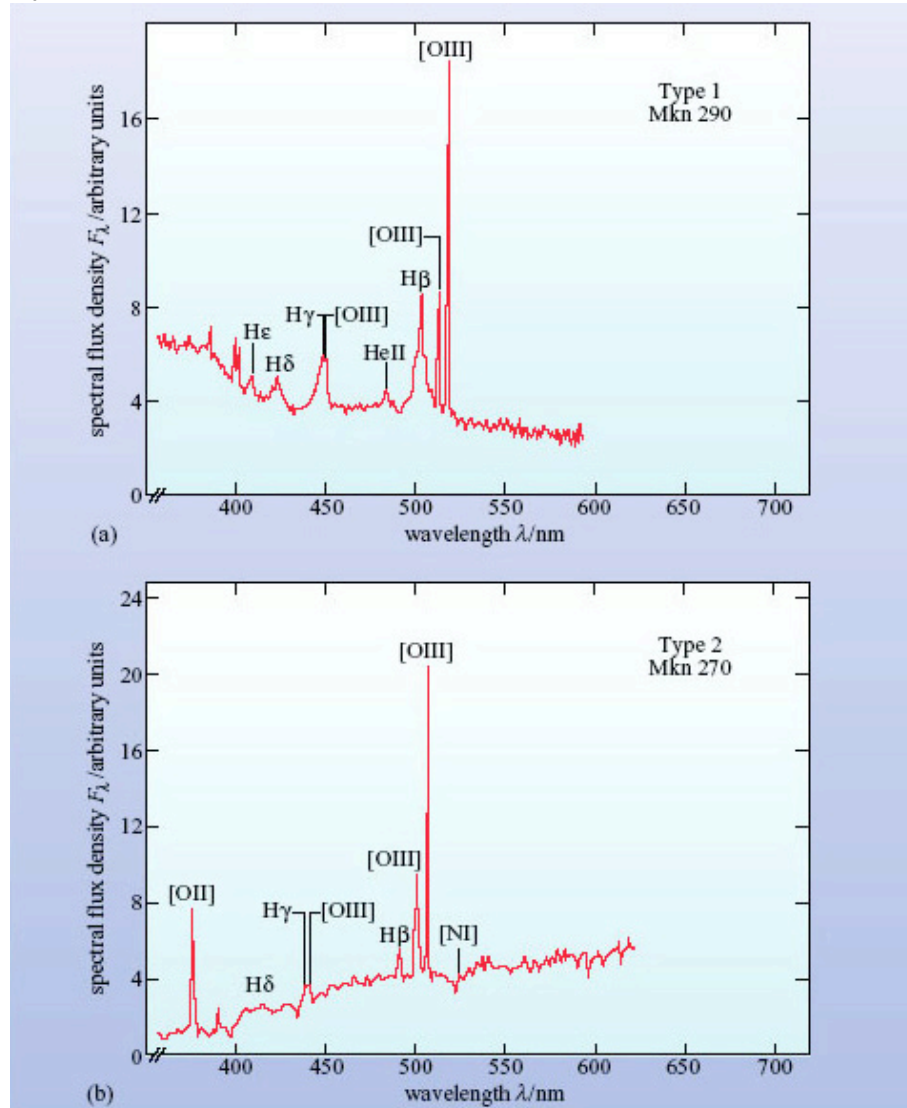
density gas, collisions are rare and de-excitation via photon emission is more likely (Gray & Corbally, 2009). Thus, forbidden lines are the signature of a low-density environment and are usually denoted by square brackets, for example [O III], meaning a forbidden line produced by doubly ionized oxygen.

4.1 Spectra of Seyfert Galaxies

The accepted division of Seyferts into Sy1 and Sy2 types was first proposed by Khachikian and Weedman (1974), based on the presence (Sy1) or absence (Sy2) of broad bases on permitted emission lines. Some representative spectra are shown in Figure 7, with an Sy1 example in the upper graph and an Sy2 galaxy in the lower. Narrow lines are present in both Sy1 and Sy2 galaxies and consist of forbidden lines, especially [O III]. Note that even the narrow lines in Seyfert galaxies are broader than the emission lines in non-AGN galaxies, and have speeds of around 500 km s^{-1} . However, the $H\beta$ and $H\delta$ permitted lines are characteristically broadened in Sy1 compared to Sy2, with speeds of up to 10^4 km s^{-1} (Peterson, 1997).

As regards Seyferts intermediate between Sy1 and Sy2, type 1.5 is defined by H I composite emission line profiles where a narrow line is superimposed on a broad line. Galaxies where the narrow $H\alpha$ and $H\beta$ lines are strong, but broad lines are weak, are known as Type 1.8, and those with a weak $H\alpha$ component but no $H\beta$ are designated Type 1.9 (Osterbrock & Ferland, 2006).

Figure 7: Spectra of Sy1 (Upper) Sy2 (Lower) Galaxies Compared
 $H\beta$ and $H\delta$ lines are more prominent and broader in Sy1, and narrower in Sy2



Source: Blandford, R.D. et al. 1990, *Active Galactic Nuclei*, 59

4.2 Spectra of Quasars

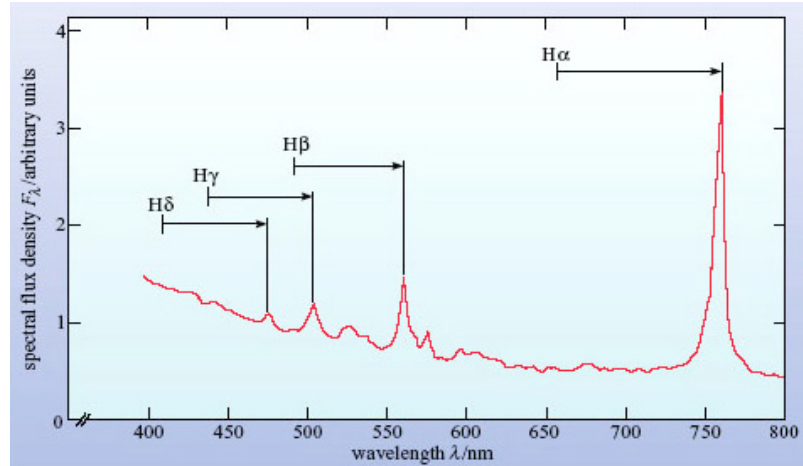
The characteristic broad emission line spectrum of a quasar is shown in Figure 8 (Upper). Figure 8 (Lower) is a composite spectrum assembled from several hundred quasars.

Figure 8 (Upper): Spectrum of Quasar 3C 273

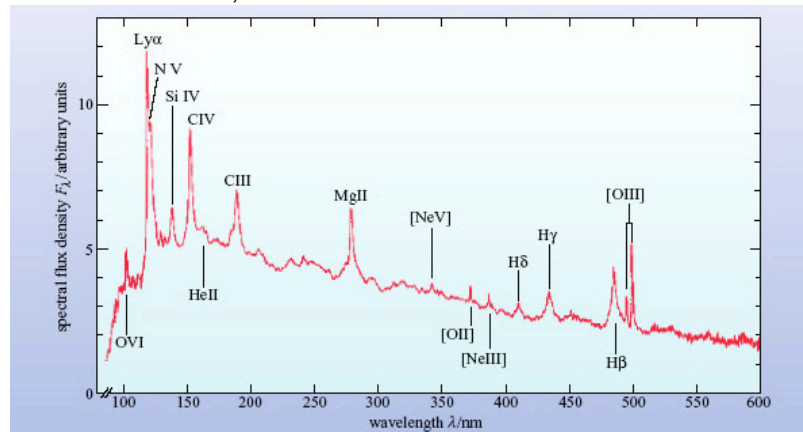
The arrows indicate the redshift from the at-rest wavelength; $z=0.158$, distance 650Mpc^[4]

Figure 8 (Lower): Composite Quasar Spectrum (Average for 700 Quasars)

Wavelength normalized to at rest values



Source: Kaufmann, 1979



Source: Peterson, 1997

As we have previously noted, radio quiet quasar spectra bear considerable similarity to Sy1 galaxies. However, quasar narrow lines are weaker relative to the broad lines than is the case in Seyferts (Peterson, 1997).

Unlike the Seyfert galaxies, stellar absorption lines are generally absent in quasars (Jones & Lambourne, 2003). This can be attributed to their distances, which typically exceed that of the Seyferts by a factor of $>10^2$.

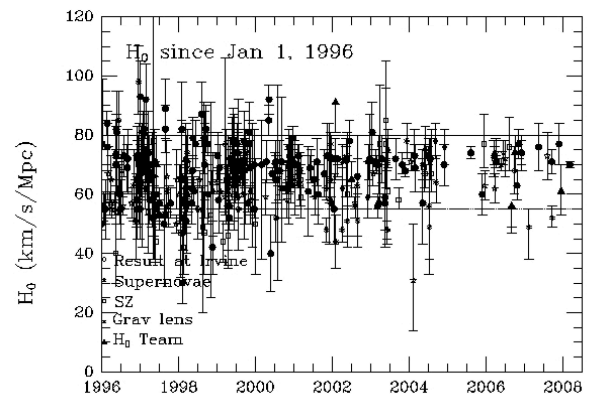
[4] Redshift (z ; see also footnote [3]) and distance (d) are related by:

$$z = \frac{H_0}{c} d \quad (4.2.1)$$

(Jones & Lambourne, 2003)

where H_0 is the *Hubble constant* and c the speed of light. H_0 is a constant of proportionality expressing the rate at which the universe is expanding in the current epoch. It may be defined as $H_0 = v/d$ (or $v = H_0 d$), where v is the recessional velocity (Sparke & Gallagher, 2007). The spread of measured values since 1996 is plotted in Figure 9, which indicates a central value of about $72\text{-}73\text{km s}^{-1}\text{Mpc}^{-1}$.

Figure 9: Measured Values of H_0 Since 1996



Source: www.cfa.harvard.edu

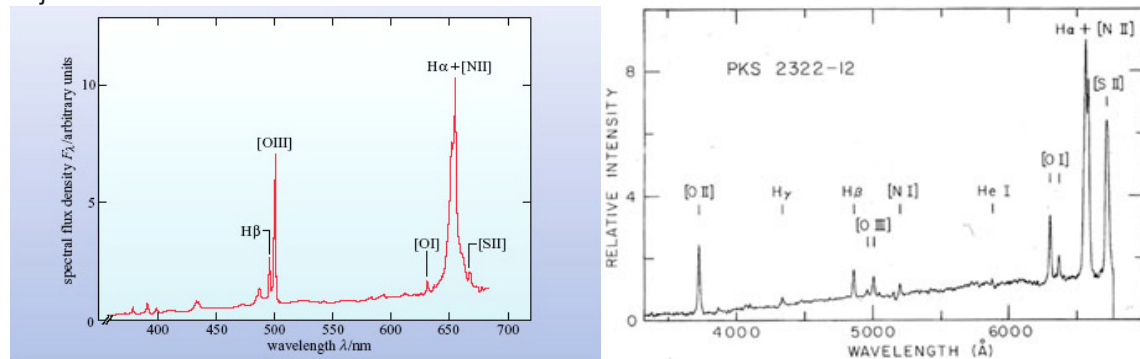
4.3 Spectra of Radio Galaxies

The spectrum of the broad line radio galaxy 3C 445 is shown in Figure 10, Left. It contains an especially broad Balmer ($H\alpha$) permitted line with a speed of $1.4 \times 10^4 \text{ km s}^{-1}$ although the speed can be twice as high in some radio galaxies (e.g. 3C 382). The Balmer lines are asymmetric and have “unusually steep decrements” (Osterbrock, 1976). There are a number of narrower forbidden lines, those of [OIII] and [NII] being especially intense. The narrow line galaxy PKS 2322-12 (Figure 10, Right) exhibits a superficially similar spectrum, but the Balmer lines have much lower speeds while the [O I], [O II] and [S I] lines are considerably more intense. Absorption lines are also detectable, separating them from the quasars.

Figure 10 (Left): The Broad Line Radio Galaxy 3C 445

Figure 10 (Right): Narrow Line Radio Galaxy PKS 2322-12

adjusted to zero redshift



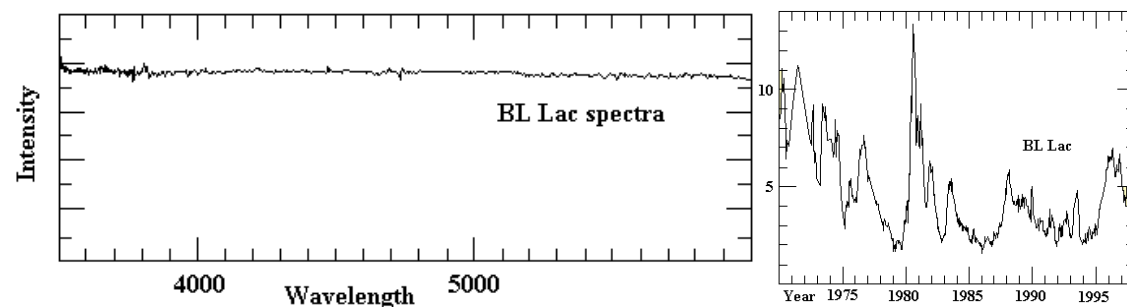
Source: Osterbrock et al. 1976 and Osterbrock, 1978

4.4 Spectra of Blazars (BL Lacs and OVV)

BL Lac objects are luminous across all electromagnetic wavelengths, but the light is a polarized, non-thermal continuum and the spectra are essentially featureless (Figure 11, Left). There are no emission lines and at most a small number of weak absorption lines. As we shall see in Section 6, this is thought to arise from the unusual viewing angle. The mouth of the blazar jet is directed precisely towards Earth, obliterating almost all other features from the observable spectrum of the host galaxy. As we have seen, the BL Lacs were originally believed to be variable stars. Their visual appearance is stellar and they exhibit periodic substantial fluctuations in brightness (Figure 11, Right). OVV spectra share with the BL Lacs qualities such as light polarization and abrupt variability, but feature strong emission lines (Emerson, 1999).

Figure 11 (Left): Featureless BL Lac Spectrum

Figure 11 (Right): Plot of BL Lac’s Variable Luminosity



Source: www.uni.edu/morgans/astro/course

5. The Central Engine: an SMBH as a Mechanism to Power AGN

We have seen that the energy output of an AGN is in the range 10^{40} - 10^{47} erg s^{-1} . Given the Sun's bolometric luminosity (L_{\odot}) is 3.8×10^{33} erg s^{-1} (Kutner, 2003), an AGN emits approximately 2.5×10^6 - 10^{13} L_{\odot} , i.e. up to 25 trillion times more energy. We examine here the physics by which the AGN generate their prodigious output, and begin by examining the evidence for SMBH in galaxy cores.

5.1 Evidence for SMBH Existence in Galaxy Cores

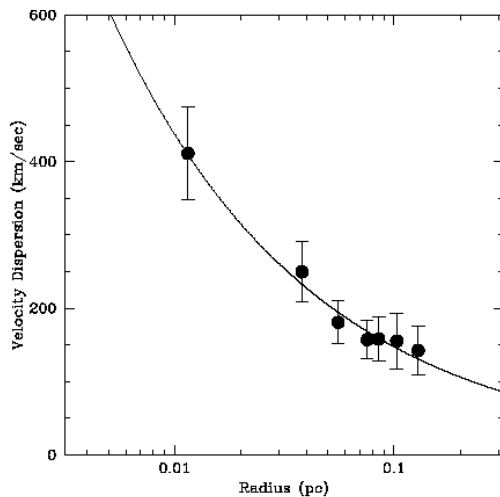
One immediate constraint on any proposed model is the small size of the emitting region. AGN luminosity is variable, sometimes over only a few hours (Sparke & Gallagher, 2007). The radius (r) of the AGN is constrained by the speed of light (c) and the period of variability (Δt) such that:

$$r \leq c\Delta t \quad (5.1.1)$$

since an object whose output varies cannot be larger than the distance light travels in the period of variability. The equation gives an upper limit of 2.6×10^{13} m (173AU) in the case of an AGN with a period of one day, and some AGN periods are significantly shorter than this. We must therefore explain the energy output within a zone comparable to the size of the Solar System, and typically $>4 \times 10^7$ times smaller than an AGN host galaxy.

There is now abundant evidence that an SMBH resides at the centre of most large galaxies, including the Milky Way. In the Milky Way's case, a Keplerian ($1/r^{1/2}$) decline in the velocity dispersion of stars observed in close orbit around the galactic centre is indicative of a dominant, point-like central mass (Ghez, 1998) (Figure 12).

Figure 12: Velocity Dispersion of Stars in the Milky Way Central Cluster



Source: Ghez et al., 1998

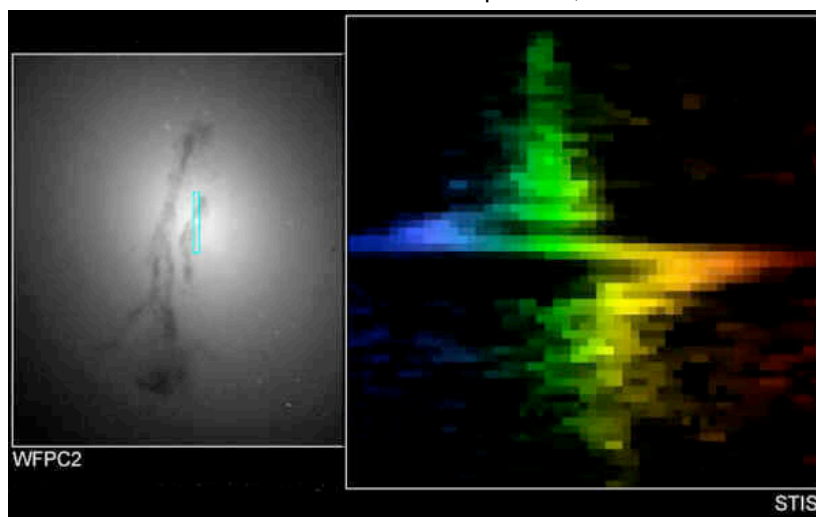
When a star's orbital period (P) and semimajor axis (a) have been determined, the combined mass of the central mass (M_1) and the orbiting star (M_2) is given by the Newtonian form of Kepler's Third Law, where G is the gravitational constant:

$$M_1 + M_2 = \frac{4\pi^2}{G} \frac{a^3}{P^2} \quad (\text{Ostlie \& Carroll, 2007}) \quad (5.1.2)$$

As $M_1 \gg M_2$, the solution is effectively the mass of the central object. Stellar kinematics of 28 stars in the centre of the Milky Way have now been determined to high precision (Eisenhauer, 2005, Ghez, 2008; Gillessen, 2009). The Galaxy's central mass is generally accepted to be about $4.3 \times 10^6 M_{\odot}$, with a radius <125 AU, corresponding to the pericentre distance of one of the stars (S2) in close orbit (Schödel, 2002).

Miyoshi (1995) used very long baseline radio interferometry (VLBI) and water maser^[5] emission to measure the speed and orbital period of gas near the centre of the galaxy NGC 4258. The central mass was determined to be $3.6 \times 10^7 M_{\odot}$ and its density $>4 \times 10^9 M_{\odot}/pc^3$ (Moran, 1995). Another method used to detect central black holes is the spectral analysis of emission lines by the HST. One example is M84 (Figure 13). The measured velocity of $370 km s^{-1}$ indicates a central mass of $1.5 \times 10^9 M_{\odot}$ (Bower et al. 2000).

Figure 13 (Left): Core of M84, Where the Suspected SMBH is Located
Figure 13 (Right): Rotational Motion of Stars/Gas Along the Spectroscopic Slit
 The change in wavelength indicates whether an object is moving toward (blue) or away (red) from the observer. If no black hole were present, the line would be vertical across the scan.

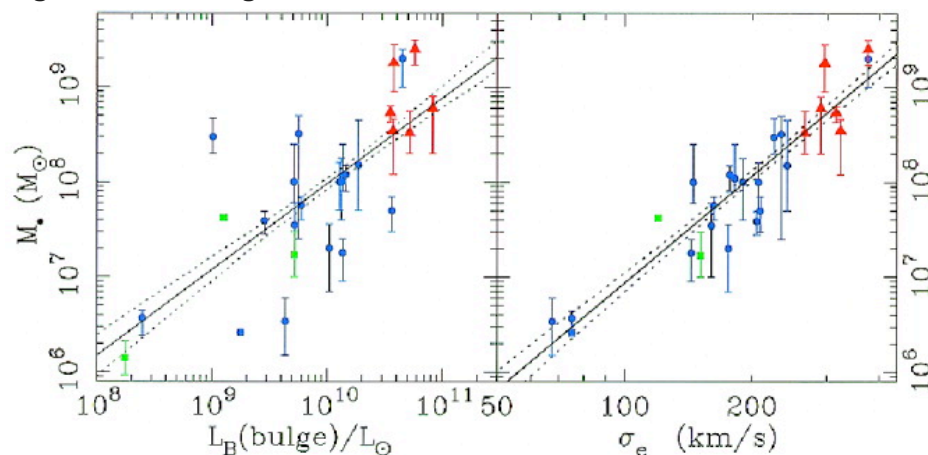


Source: Bower, G. A. & Green, R. F. (NOAO)

5.2 The Scaling Relation for SMBH

It is now well established that bigger galaxies have bigger black holes (Kormendy & Richstone, 1995; Magorrian (1998), Gebhardt et al. 2000; Merrit & Ferrarese, 2001; Bandara et al. 2009) and this *scaling relation* is illustrated in Figure 14. The left chart plots the SMBH mass (M_{\bullet}) in terms of solar masses (M_{\odot}) against galaxy bulge luminosity in terms of solar luminosities (L_{\odot}), while the right chart is plotted against velocity dispersion (σ_e).

Figure 14: Scaling Relation for SMBH



Source: Gebhardt et al. 2000

[5] *Masers* are longer wavelength, monochromatic, coherent electromagnetic radiation produced by a cascade of atoms undergoing transition to a lower energy state. To maintain the emission, the atoms must be continually re-energized (“pumped”) back into their higher state by an energy source such as an accretion disc around a black hole.

Ferrarese & Merritt (2000) express the relationship between SMBH and the velocity dispersion (σ) of the host galaxy bulges as:

$$M_{BH} \propto \sigma^\alpha \quad (5.2.1)$$

where the exponent $\alpha = 4.8 \pm 0.5$. The scaling relationship is important in the context of AGN since many occur in high-mass elliptical galaxies, which consequently have higher mass SMBH and a powerful “engine” (see 5.3 below).

5.3 Energy Production by an SMBH

We have seen that AGN energy production takes place within a small volume of space and it has been shown beyond reasonable doubt that most large galaxies harbour an SMBH. The idea that black holes could account for the energy output of the quasars was first proposed in influential papers by Salpeter (1964) and Lynden-Bell (1969). Let us now consider the physics of the process.

The *event horizon* of a black hole is the radius from its centre at which $v_{esc} > c$. Inward of this radius, no information, including light, can escape. This radius is known as the *Schwarzschild radius* (R_s) and for a black hole of mass M is given by:

$$R_s = \frac{2GM}{c^2} \quad (\text{Kutner, 2003}) \quad (5.3.1)$$

Although no energy can be obtained from mass inward of the R_s , energy may be extracted by material falling towards it. If the in-falling material has mass m , the maximum extractable energy (E_{max}) is thus the negative of the gravitational potential energy at R_s , namely:

$$E_{max} = \frac{GMm}{R_s} \quad (\text{Kutner, 2003}) \quad (5.3.2)$$

Substituting equation 5.3.1 into 5.3.2, we obtain the highly significant result that fully half the rest-mass energy of infalling material can be extracted, as per equation 5.3.3. This mechanism is thus extremely efficient at producing energy: even stellar nuclear fusion reactions release energy at only around $0.007mc^2$ (Shankar, 2009).

$$E_{max} = \frac{GMm}{R_s} \therefore E_{max} = \frac{GMm}{2GM/c^2} = \frac{mc^2}{2} \quad (5.3.3)$$

We may now proceed to estimate the potential luminosity (L_{max}) of an SMBH at a given *mass accretion rate*. The quantity m in equation 5.3.3 is thus substituted for the change in mass over the time period (dm/dt). If we simulate the accretion of one solar mass (2×10^{33} g) per year (3.15×10^7 s) and take c as 3×10^{10} cm s⁻¹, we obtain:

$$L_{max} = \frac{(dm/dt)c^2}{2} = \frac{(2 \times 10^{33} \text{g} / 3.15 \times 10^7 \text{s})(3 \times 10^{10} \text{cm})^2}{2} = 2.8 \times 10^{46} \text{ erg s}^{-1} \quad (5.3.4)$$

It should be added that in practice energy production does not reach the theoretical calculated value ($1/2mc^2$) in equation 5.3.3 because mass does not fall directly into the hole, but through a decaying orbit in an accretion disc mediated by disc viscosity (Sparke & Gallagher, 2007). The actual energy extracted is given by ηmc^2 , where η may be regarded as a function of the SMBH spin rate and has value of ~ 0.06 - 0.4 (Narayan & Quataert, 2005). Nevertheless, the process remains substantially more efficient than stellar nuclear fusion and is the most efficient source of power known in the universe other than matter-antimatter annihilation. We may accordingly conclude that the accretion of approximately $1M_\odot \text{yr}^{-1}$ is adequate to explain the observed luminosity of a moderately bright AGN, while the most luminous require $\sim 10^2 M_\odot$ (Frank et al. 2002).

5.4 Constraints on AGN Luminosity: The Eddington Limit

An AGN cannot accrete fuel without limit because its luminosity (L) creates an outward pressure on orbiting electrons due to *Thomson scattering*^[6]. (Scattering by protons is much less efficient due to their higher mass). Should this pressure exceed the inward pull of gravity, the supply of fuel to the nucleus is terminated and the AGN “turns off”. The balance between inward gravitational attraction (the left side of equation 5.4.1) for a black hole of mass M and the outward force on a spherically symmetrical object (right side of equation 5.4.1) can be expressed in terms of the standard Newtonian gravitational equation as:

$$\frac{GM(m_e + m_p)}{r^2} = \frac{\sigma_T L}{4\pi r^2 c} \quad (\text{Sparke \& Gallagher, 2007}) \quad (5.4.1)$$

where σ_T is the cross section of the electrons in fully ionized hydrogen. Complete ionization is a reasonable working assumption given the temperatures in accretion discs around SBMH. The quantities m_e and m_p are the masses of the electrons and protons in the orbiting gas respectively, although in practice the quantity m_e is small compared with m_p and can be ignored for most purposes.

Using the fact that the two expressions in equation 5.4.1 are equal, we can solve for the maximum luminosity, known as the *Eddington limit* (L_E), at which the SMBH may continue to accrete fuel. The answer may alternatively be expressed more conveniently in terms of solar luminosity:

$$L_E = \frac{4\pi GMm_p c}{\sigma_T} \approx 3 \times 10^4 \frac{M}{M_{Solar}} L_{Solar} \quad (5.4.2)$$

The Eddington limit for an SMBH of $10^9 M_\odot$ would thus be approximately $3 \times 10^{13} L_\odot$.

5.5 Availability of AGN Fuel

We have noted a typical AGN fuel requirement of $1M_\odot \text{yr}^{-1}$, and a reservoir of some $10^8 M_\odot$ may be needed to sustain an AGN over its entire life. This corresponds to ~10% of the available cold gas in a typical spiral galaxy (Gallimore et al. 2010). Cold gas (<1000K) accretes more easily than hot gas because the former does not resist collapse (Gunn, 1979).

Nevertheless, the precise mechanism by which fuel is brought to the SMBH remains poorly understood. In lower luminosity AGN, the fuel is most probably contained within the ISM of the host galaxy itself, and the principle unresolved problem is how to remove angular momentum (to one part in 10^7) in order to bring the gas from kpc distances to the event horizon on AU scales (Martini, 2004). Non-axis symmetric features such as bars on kpc to pc scales can promote the inward flow of gas to the nucleus (Schwarz, 1981; Shlosman, 1994).

[6] When an electromagnetic wave strikes a charged particle, energy is absorbed by the particle and re-emitted as electromagnetic radiation. The process is equivalent to the scattering of the electromagnetic wave by the particle and is known as *Thomson scattering*. The effect is reduced by a factor of 3×10^6 in protons due to their higher inertia (and thus greater ability to absorb the incident energy) (Peterson, 1997). For an electron, the Thomson scattering cross section (σ_T) is related to the *classical electron radius* ($2.8 \times 10^{-15} \text{m}$) by:

$$\sigma_T = \frac{8\pi}{3} (2.8 \times 10^{-15} \text{m})^2 = 6.65 \times 10^{-29} \text{m}^2 \quad (\text{Fitzpatrick, 2002}) \quad (5.4.3)$$

Thomson scattering applies only to interactions with low energy photons ($v \ll mc^2/h$), where h is the Planck constant. If photon energy is equal to or greater than the electron energy, quantum physical effects must be taken into account and the process becomes known as *Compton scattering* (Flynn, 2005).

Some 50-80% of disc galaxies are thought to contain *nuclear spirals* in their inner regions (Pogge & Martini, 2002), which are density waves generated in gas by a rotating potential. Spiral shocks generated in these waves by the SBMH can channel gas to the galaxy core (Maciejewski, 2004). For higher luminosity systems, galaxy interactions and their concomitant tidal effects are likely to drive gas inward from the galactic disc (Toomre & Toomre, 1972; Hernquist, 1989; Barnes & Hernquist, 1992).

6. The Morphology of AGN and Unification Theory

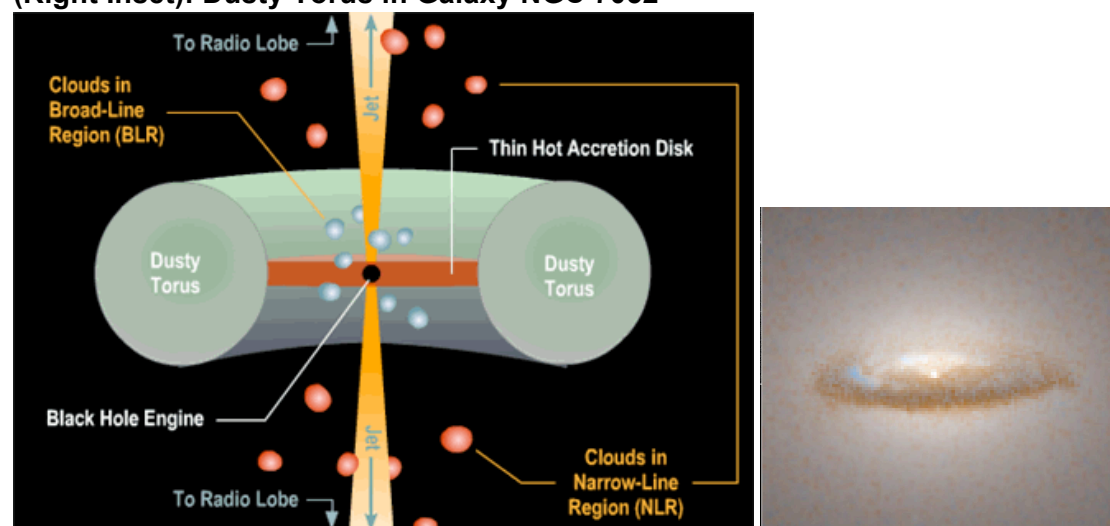
We now proceed to examine the detailed structure of an AGN and review the *unified model*, which attempts to explain the various AGN phenomena within a single, overarching framework. The discussion is in five parts, dealing with the inner core, the accretion disc, dusty torus, the long range radio jets and the finally the unified model itself. The discussion of unification is based around the framework proposed by Antonucci (1993) and Urry & Padovani (1995), and incorporates work on Seyfert galaxies by Antonucci & Miller (1985).

6.1 The Inner Core of AGN

The proposed structure of the inner core of an AGN is presented in Figure 15. An SMBH is the only known mechanism able to generate sufficient energy to power AGN luminosity, and it must be fed by gas to sustain output. Infalling gas has angular momentum, which results in a thin, rapidly rotating *accretion disc* of material forming around the black hole (see 6.2 below). Material in the disc slowly spirals into the black hole and is heated to high temperature as it experiences progressively greater gravitational forces. Increasing temperature causes radiation at the full range of wavelengths, resulting in the intense observed luminosity of an AGN.

High velocity gas clouds in the immediate vicinity of the disc (typically to around ~100 light days) are known as *broad line region* (BLR) clouds and give rise to the characteristic Doppler broadened emission spectra discussed earlier. At ~30pc, the BLR is surrounded by a *dusty torus*, which obscures the BLR at low viewing angles, and accounts for the lack of broad line spectra in some AGN. The presence of the torus was originally inferred on theoretical grounds to explain absence of the broad emission lines, but observational evidence now also exists in the HST image of the central region of NGC 7052 (inset, Figure 15). Moving outward from the torus to ~300pc, the lower velocity *narrow line region* (NLR) clouds generate the narrow emission lines of AGN.

**Figure 15: Inner Structure of an AGN (not to scale)
(Right Inset): Dusty Torus in Galaxy NGC 7052**

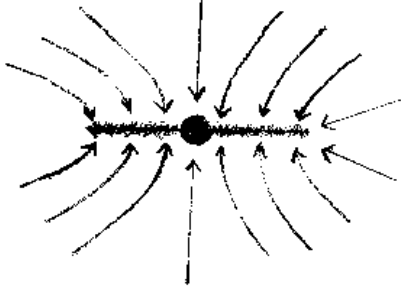


Source: Astronomy online.org and HST image (released 22 June 1998)

6.2 The Accretion Disc

The accretion disc is formed by gas flowing from all directions towards the SBMH, and the gas' motion inevitably imparts angular momentum to it. Matter under these conditions will always evolve towards a thin disc configuration orientated in the plane of the rotational axis: flow parallel to the rotation axis is unimpeded by rotation, but flow toward the center in the equatorial plane is prevented by rotation (Figure 16). The phenomenon is widely observed in the universe, not only around black holes, but also in proto-planetary discs and stellar accretion discs.

Figure 16: Inflow to the Equatorial Plane of an Accretion Disc



Source: fti.neep.wisc.edu

In order to feed the black hole, the disc's angular momentum must somehow be transferred outward, allowing material in the inner disc to fall into the event horizon. The crucial factor mediating outward transport and the conversion of rotational energy to thermal energy is *disc viscosity* (Narayan & Quataert, 2005). The physics of the process have proved a major challenge to theorists for many years, but it is believed to be magnetic in origin and two mechanisms have been proposed. Blandford & Payne (1982) suggested *magnetohydrodynamic (MHD) outflow*, whereby magnetic fields generate torques in the disc and carry away angular momentum in the outflow. The second is *magnetic turbulence* due to the differential rotation of annuli of material at varying distances from the SBMH. The disc contains ionised gas, allowing free electrons to interact strongly with local magnetic fields. Differential rotation stretches the field lines until they form loops inside and outside the radius of orbiting material, causing it to break up into individual bubbles. This disrupts smooth orbital flow, increasing viscosity and turbulence, and is known as *Balbus-Hawley instability* (Stone et al. 1996, Balbus & Hawley, 1991 & 1998).

6.3 The Torus, Dust and Infrared Emission

Infrared emissions are detected from many AGN and are explained as radiation by dust particles in the torus. High-energy (UV and X-ray) photons emitted from the accretion disc heat the dust grains, which re-radiate at a peak wavelength (λ_{peak}) in accordance with Wien's displacement law:

$$\lambda_{peak} = \frac{2.9 \times 10^{-3} mK}{T} \quad (\text{Ostlie \& Carroll, 2007}) \quad (6.3.1)$$

where T is the temperature in kelvins.

As dust vaporizes at $>2000K$, the torus must be far enough from the accretion disc to keep the temperature below this value. The flux density (L) at a distance r from an SMBH is thus $L/4\pi r^2$ and the radiation intercepted/absorbed (R_i) by a dust grain of radius a is:

$$R_i = \pi a^2 \frac{L}{4\pi r^2} = \frac{La^2}{4r^2} \quad (\text{Jones \& Lambourne, 2003}) \quad (6.3.2)$$

The temperature of the dust grain will rise until radiation it emits across its surface equals the intercepted radiation. Assuming a spherical dust grain is radiating as a

black body evenly across its surface, this emitted radiation is given by the Stefan-Boltzmann law ($L=4\pi a^2\sigma T^4$, where σ is the Stefan-Boltzmann constant) therefore:

$$4\pi a^2\sigma T^4 = \frac{La^2}{4r^2} \text{ and therefore } r = \left(\frac{L}{16\pi\sigma T^4}\right)^{1/2} \quad (6.3.3/6.3.4)$$

For a highly luminous AGN of 10^{47} erg s^{-1} , the distance at which dust sublimates, known as the *sublimation radius*, is 1.48×10^{16} m, or approximately 0.5pc. Using equation 6.1.1, we can see that radiation re-emitted by dust at 2000K will have a wavelength of 1.5×10^{-6} m (1500nm), in the near-infrared band. In practice, the dusty torus extends to considerably greater distances, resulting in far infrared emissions.

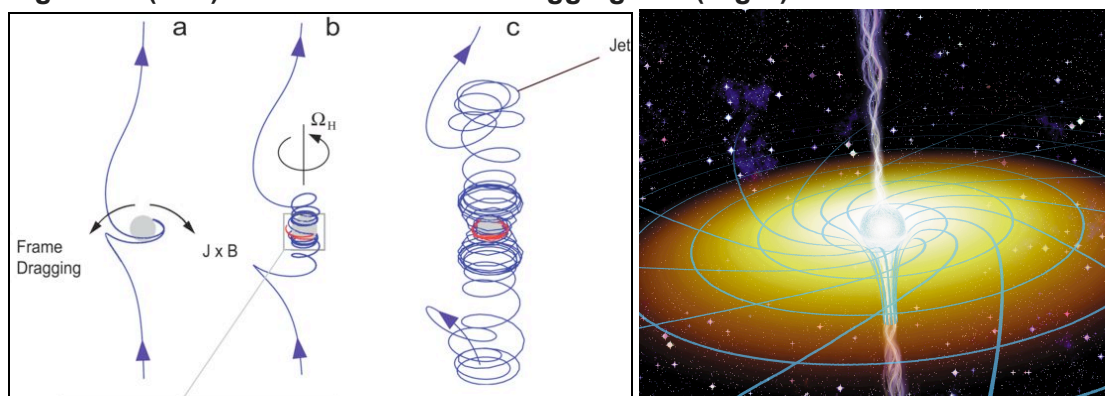
6.4 Long Range Jets in Active Galaxies

The origin of jets emitted by AGN remains poorly understood, but the energy must come either from the rotation of the black hole, or from the accretion disc (Ghosh & Abramowicz, 1997). Semenov et al. (2004) and Koide (2004) have described a theory known as gravitohydrodynamics, whereby magnetic stresses induced by the hole's gravity are released as a jet, with the ejection energy drawn from the hole's rotational energy. Jets emerge from AGN cores at relativistic speeds ($>0.95c$).

Immediately outside the black hole's event horizon is a region known as the *ergosphere* where space-time is forced to co-rotate with the hole by the intense gravitational field. This is known as *frame dragging* and Figure 17 (Left) shows a computer simulation (Narayan & Quataert, 2005). Magnetic field lines are pulled forward in the direction of the black hole's spin (Figure 17a), becoming progressively more wound over time (Figure 17b/c) and forming two opposing channels through which magnetized plasma in the ergosphere may be ejected. The black hole spin vector is labeled Ω_H , and the electric and magnetic field vectors are marked J and B respectively.

AGN jets are extremely narrowly collimated and inject energetic particles and magnetic fields into radio galaxy lobes (Figure 17, Right). The result is the characteristic bi-polar structure of Cygnus A (refer to Figure 4, Right) and other radio loud AGN (Burke & Graham-Smith, 2010).

Figure 17 (Left): Relativistic Frame Dragging and (Right) AGN Jet Production



Source: Narayan & Quataert, 2005 & NASA Science News

6.5 Doppler Brightening and Superluminal Motion

If the jets described above are observed close to pole-on (radio loud quasars are thought to be orientated at this angle, see 6.6), and matter is being ejected at relativistic speeds (Blandford et al. 1977), then the radiation within the jet will be beamed along the jet's axis, increasing its intensity in an effect known as *Doppler brightening* (or boosting) (Burke & Graham-Smith, 2010). Conversely, a jet pointing away from the observer is *Doppler attenuated*, and may be faint or unobservable, giving the impression of a one-sided/asymmetric object.

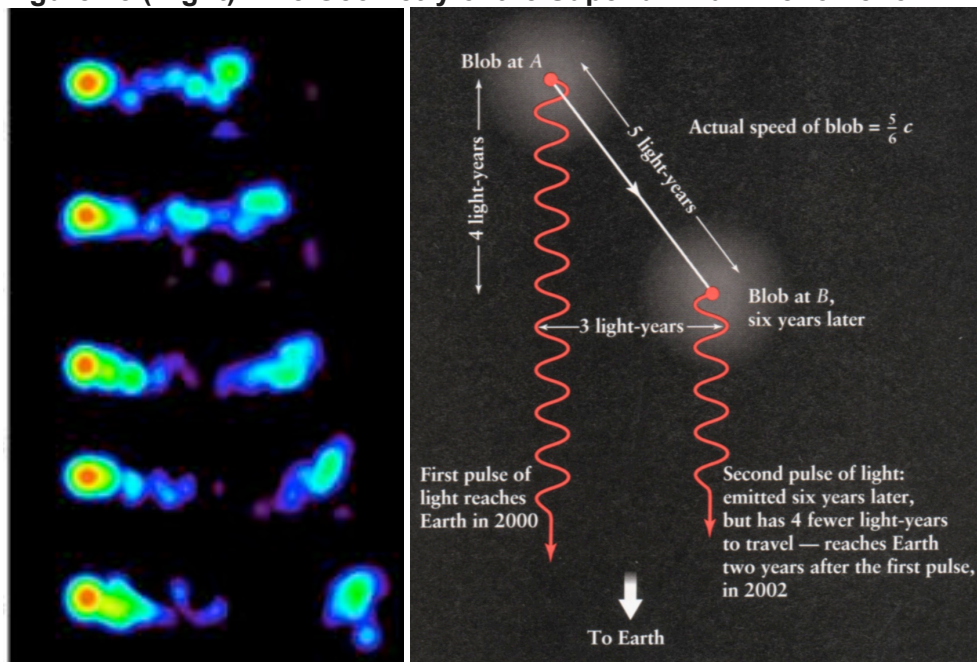
Superluminal motion refers to a phenomenon in which an object appears to be traveling faster than light speed (c) to a distant observer. It was predicted as a theoretical possibility by Rees (1966), and subsequently confirmed observationally by Pearson et al. (1981). It is important to be aware of both Doppler brightening and superluminal motion when considering the unified theory for AGN, as the discovery of superluminal motion led to the insight that viewing angle is important when interpreting AGN.

An example of superluminal motion can be seen in Figure 18 (Left). The quasar 3C 279 is shown in a time series of images beginning in 1992 at the top 1998 at the bottom (Piner et al. 2003). The quasar's core is the red circular zone on the left, while the blue area on the right is a jet emitted by the quasar's AGN. The angular separation between the quasar core and the jet increases over the six-year period by an amount corresponding to 20 light years (6.1 pc) at 3C 279's distance. The jet thus appears to have traveled 20 light years in only six years of time. At first, this was taken to be an error in the quasar's distance, but the observation can be explained at the previously determined distance without violating special relativity.

Figure 18 (Right) sets out the geometry of the phenomenon, which can be modeled as a Pythagorean right-angled triangle. The most familiar 3-4-5 unit triangle is used here. The quasar is moving, but can be thought of as stationary relative to the jet, which is approaching Earth at a high fraction ($5/6$) of the speed of light. After six years, the jet travels five light years along the hypotenuse of the triangle, but appears from an Earth perspective to have traveled three light years along the triangle's lower side. The jet is, however, now four light years closer to Earth, so a signal actually emitted six years later arrives at Earth only two years later, creating the impression that the jet has moved a distance of three light years in only two years. Its true speed, however, remains $5/6c$.

Figure 18 (Left): Superluminal Motion in Quasar 3C 279

Figure 18 (Right): The Geometry of the Superluminal Phenomenon



Sources: NRAO, Piner et al. (2003) crab0.astr.nthu.edu.tw

Most real-world observations of superluminal motion involve even higher speeds only fractionally below c , and smaller angles to the line of sight, so apparent speeds can exceed c by a larger margin than in the above example. The apparent velocity (v_{app}) relative to the true velocity (v) is given by:

$$\frac{v_{app}}{v} = \frac{1}{(1 - \beta^2)^{1/2}} \quad (\text{Kutner, 2003}) \quad \text{and therefore} \quad v_{app} = \frac{v}{(1 - \beta^2)^{1/2}} \quad (6.5.1/6.5.2)$$

where β is the cosine of the angle between the line of sight and the jet's trajectory. It will be noted that equation 6.5.2 takes the form of the *Lorentz transformation* in special relativity, where:

$$\gamma = \frac{1}{\sqrt{1 - (v/c)^2}} \quad (\text{and } v/c = \beta) \quad (6.5.3)$$

The solution to equation 6.5.2 is consequently known as the *Lorentz factor*. If $v=0.95c$ and the angle of the jet's trajectory is 8° ($\cos = 0.99$), then $v_{app} = 6.7c$.

6.6 The Unified Model: AGN Type as a Function of Viewing Angle

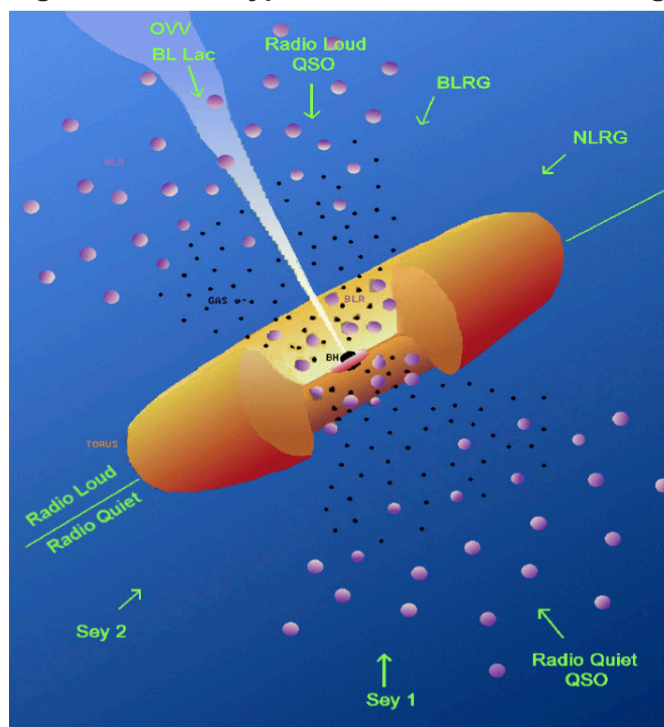
A number of considerations lend support to the notion that AGN are the same underlying physical phenomenon, differing only in the viewing angle (since AGN are axisymmetric) and in luminosity (most likely a function of SMBH mass). Among the radio quiet galaxies, we have already noted the spectral similarities between radio quiet quasars and Sy1 galaxies. Moreover, Antonucci & Miller (1985) observed NGC1068 (an Sy2 galaxy) in polarized light and found a Sy1 spectrum containing broad emission lines. They accordingly proposed a unified model for the Seyferts.

Within the radio loud AGN group, broad line radio galaxies and radio loud quasars have much in common spectroscopically. Barthel (1989) proposed additionally that FR II radio loud galaxies (quasars and narrow line radio galaxies, which at first sight appear spectroscopically distinct) could be unified if the quasar nucleus were hidden by optically thick material, such as a dusty torus.

The fact that FR I radio galaxies have only weak and narrow emission lines, and BL Lacs spectra are essentially featureless, has prompted models for unification (Antonucci & Ulvestad, 1985; Padovani & Urry, 1991) under which BL Lacs are the beamed cores of FR I radio galaxies.

The short-term (~ 0.1 yr) variations observed in broad lines such as $H\alpha$ and $H\beta$ contrast with the minimal variability of the narrow lines, and suggest that broad and narrow lines originate in different physical regions of the AGN, as proposed by unified models. Figure 19 plots the viewing angles for the various AGN sub-types as proposed by current unification theory.

Figure 19: AGN Types as a Function of Viewing Angle



AGN can be classified based on whether the inner, broad line region (the small black dots in Figure 19) is visible from Earth. This requires a higher viewing angle. At low viewing angles, only the narrow line (larger pink dot) region can be seen.

Radio quiet AGN occur in galaxies without jets, and radio loud AGN arise in those with the jets. (Figure 19 is a hybrid diagram to permit both types to be depicted).

Source: Adapted from Urry & Padovani (1995)

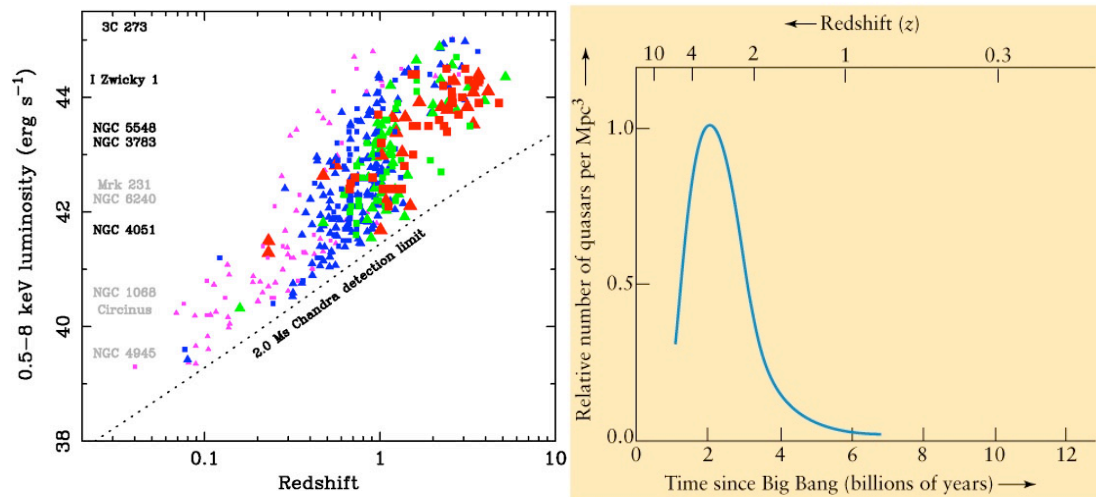
7. The Evolution of AGN

The distances and luminosities of AGN provide strong clues to their evolutionary path. It has been shown that quasar luminosity function increases with redshift (Figure 20, Left) (Boyle et al. 2000). Quasar density increases to $z=2\sim3$ (Franceschini et al. 1999), peaks near $z=3$ at a light travel time of 10^{10} years (Page et al. 1997; Miyaji et al. 2001), then falls off rapidly at higher values of z (York et al. 2000; Fan et al. 2003). Quasar density at the redshift of peak distribution is some 10^3 times greater than in the current epoch (Figure 20, Right).

Figure 20 Left: AGN Luminosity and Redshift

Luminosities at 0.5-8 keV for some local AGN are shown on the left-hand axis for comparison

Figure 20 Right: Quasar Relative Occurrence Plotted Against Redshift



Source: ned.ipac.caltech.edu and www.ualberta.ca

We observe less luminous AGN such as Seyferts (Figure 21) at smaller distances. Most nearby galaxies have quiescent (i.e. non-active/non-accreting) SBMH. This includes the Milky Way itself and M31 (Burke & Graham-Smith, 2010). We also occasionally find galaxies such as M33, another local group member, which has no central black hole or at most a low-mass hole of $3 \times 10^3 M_{\odot}$ (Merritt et al. 2001).

Figure 21: AGN Type and Luminosity Relative to the Milky Way Galaxy

Galaxy Type	Luminosity (Milky Way=1 or 2×10^{10} Solar Luminosities)
Normal	<10
Seyfert	0.5-50
Radio	0.5-50
Quasar	100-5,000

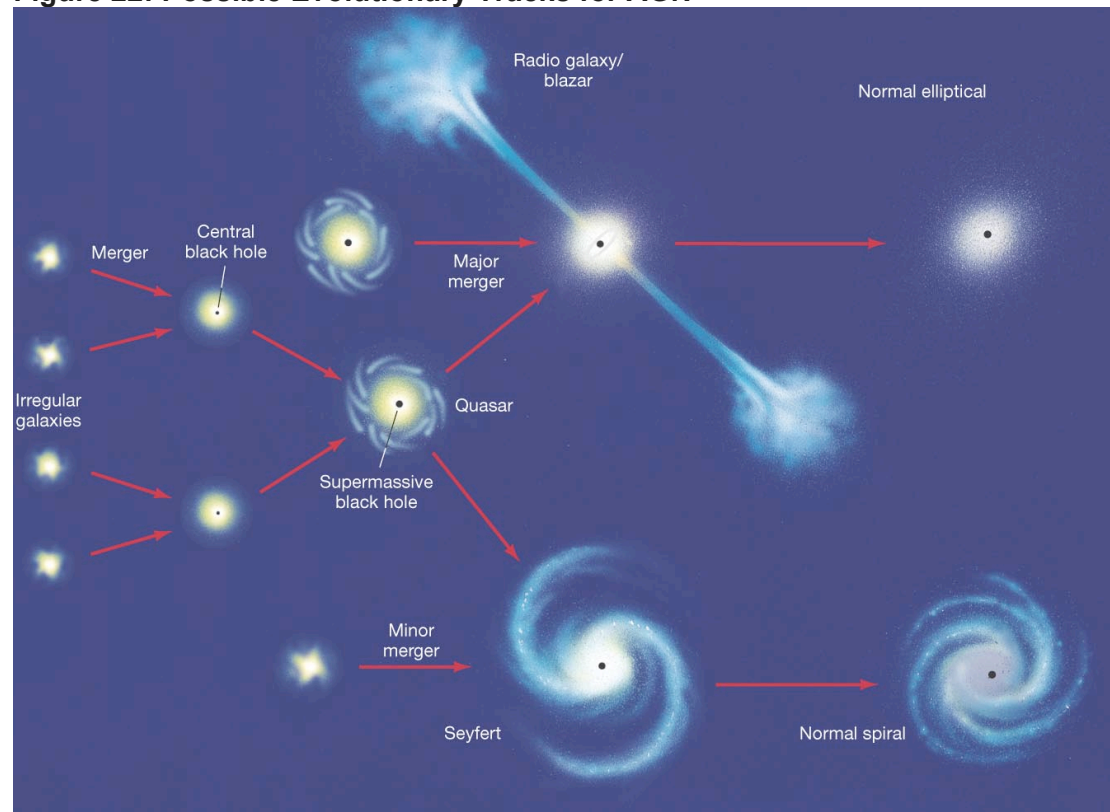
Source: cornell.edu

These findings strongly indicate that the most luminous AGN are a phenomenon of the past. Cosmologically speaking, quasars are short-lived objects that have largely depleted their fuel supply in the current epoch. A few may be rejuvenated if a new fuel source becomes available, possibly as a result of galaxy merger or *harassment* (close encounters of separate galaxies). About one percent of known galaxies are AGN. Given the estimated age of the universe (13.7Gyr), this suggests a typical AGN lifetime of $1\sim 1.5 \times 10^8$ yr.

The luminosity-distance relationship implies an evolutionary sequence from the intensely to the more moderately active AGN sub-types, namely from quasars through to lower luminosity types, with quiescent black holes and normal (non-active) galaxies the ultimate outcome once the fuel supply is depleted. We may postulate that radio quiet quasars evolve to Sy1 and Sy2 galaxies, and finally to normal spirals, while radio loud quasars evolve to radio galaxies/blazars and then to normal ellipticals (Figure 22). Figure 22 also shows that the quasars themselves may have

been formed by the hierarchical merging of smaller galaxies. Major galaxy mergers that spin up black hole rotation rates may be responsible for the radio loud galaxies and their highly collimated jets. The quiescent black holes observed in non-active galaxies today are the remnants of the universe's vigorous early history, when a more plentiful gas supply fed the SMBH.

Figure 22: Possible Evolutionary Tracks for AGN



Source: physics.uoregon.edu

8. Outstanding Issues

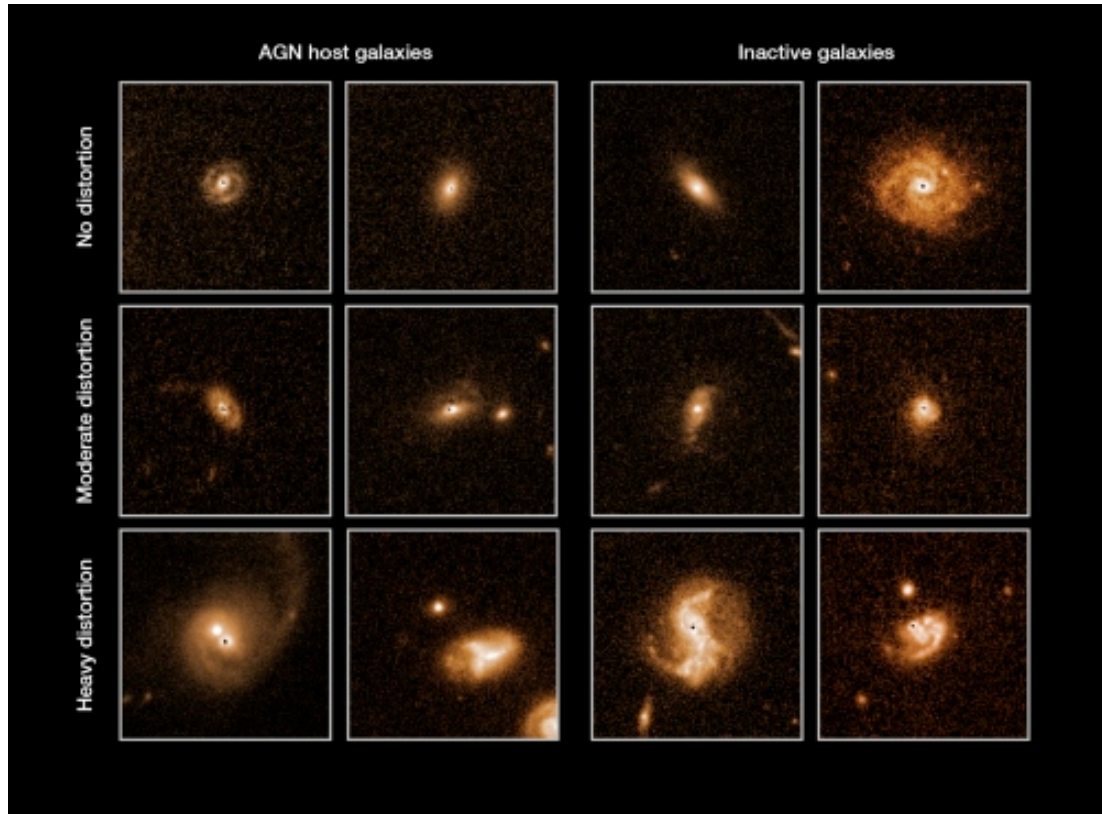
The general picture sketched in this review, namely an SMBH fuelled by an accretion disc with activity decreasing across time and key observational differences attributable to viewing angle as described by the unified model, are broadly accepted within the astrophysical community. As ever in science, however, questions remain.

Hunt & Malkan (2004) found that Sy2 galaxies have more twisted *isophotes* (lines of constant light intensity) and are more disturbed than Sy1 galaxies. The differences between the two may thus be more complex than simply the viewing angle of the central engine, and there may be evolution between the types. While Seyferts are weak radio emitters, Roy et al. (2004) found differences in radio brightness between Sy1 and Sy2 galaxies, but also proposed that the anomaly may be explicable as an optical depth effect in the narrow-line region.

Hawkins (2004) reported the discovery of a quasar in which the nucleus is viewed directly, but no emission lines are present. This would not be consistent with the unified model. The object may be an AGN in transition, i.e. in the process of being starved of fuel and shutting down.

More work is needed to understand how gas is driven into galactic cores to fuel the AGN. While galaxy mergers have long been a popular theory, a new study (Cisternas et al., 2011) using images from the COSMOS survey suggests that, while mergers are sometimes important, often they are not. A comparison of AGN and normal galaxies showed little evidence that the AGN galaxies were more disrupted (a marker of a merger) than normal galaxies (Figure 23). Galaxy harassment or gas cloud collisions within galaxies may hold the answer to this conundrum.

Figure 23: Distortion in AGN and Inactive (Normal) Galaxies Compared



Source: NASA/ESA, Cisternas (2011)

AGN radio jets and the related issue of ejection of material by the accretion disc are still poorly understood, especially in terms of jet composition, the mechanism by which matter is accelerated to relativistic speeds and even why there is a jet in some cases and not others.

Whether every galaxy has gone through an AGN phase is another area of uncertainty. The widespread presence of black holes at galactic cores and the greater availability of star-forming gas at previous epochs suggest the potential for AGN activity, but we cannot yet be sure. However, even if all galaxies have had an AGN phase, not all can achieve quasar luminosities as the SMBH in many cases is less massive than those found in quasars by a factor of 10^2 - 10^3 . However, it does seem likely that AGN are short-lived phenomena by cosmological standards.

9. Summary and Conclusions

It is still only a just over century since Edward Fath's pioneering observation of the first identified AGN, NGC 1068. The journey towards our current understanding of active galaxies has been both exhilarating and extraordinary. It has required the invention of completely new physics in the form of quantum theory and general relativity, two of the greatest intellectual achievements of the 20th century. It has been made possible by a revolution in observing technique that has opened up the entire electromagnetic spectrum, from radio astronomy through to high-energy astrophysics conducted from space. We have what appears to be a strong working model of the AGN process based on widely accepted concepts that would have stretched the bounds of credibility just a few decades ago. Much remains to be done to understand fully accretion disc angular momentum transport and jet generation in AGN, and to reconcile some of the observational findings with the unified model. However, the record of achievement to date should give us confidence that these issues will be addressed in the years ahead. Equally, there can be little doubt that new questions will emerge. The universe's most energetic phenomenon seem likely to fascinate and challenge astrophysicists for some time to come.

Acknowledgements and Dedication

The author wishes to thank Dr. Juan Madrid of Swinburne University Astronomy Online MSc degree programme for his invaluable suggestions and guidance in the preparation of this paper, and Prof. Duncan Forbes, the tutor of the MSc unit devoted to the study of galaxies. It goes without saying that the author alone accepts responsibility for any errors or inaccuracies contained herein.

He also records his appreciation to the Astronomical League and to James Schneider for their generous cooperation and support with the publication of this paper.

This paper is dedicated to my wife, Chika, and son, Andrew, for their patience and forbearance during my MSc studies, which can take up a considerable amount of time.

A full list of the references cited in this paper can be found on the following two pages.

References

- Antonucci, R.R.J. 1993, ARA&A, 31, 473-521
- Antonucci, R.R.J. & Miller, J.S. 1985, ApJ, 297, 621-632
- Antonucci, R.R.J. & Ulvestad, J.S. 1985, ApJ, 294, 158-182
- Astrobites: *Galaxy and AGN Types* website
<http://astrobites.com/glossaries/galaxy-and-agn-types/#tag> (accessed 18 Sept. 2011)
- Baade, W. & Minkowski, R. 1954, ApJ, 119, 206-214
- Balbus, S. & Hawley, J.F., 1991, ApJ, 376, 214-233
- Balbus, S. & Hawley, J.F., 1998, Reviews of Modern Physics, 70, 1-53
- Barnes, J.E. & Hernquist, L. 1992, ARA&A, 30, 705-742
- Bandara, K. et al. 2009, ApJ, 704, 1135-1145
- Barthel, P.D. 1989, ApJ, 336, 606-611
- Blandford, R.D. et al. 1977, Nature, 267, 211-216
- Blandford, R.D. et al. 1990, *Active Galactic Nuclei*, Springer-Verlag, Berlin, Germany, 6
- Blandford, R.D. & Payne, D.G. 1982, MNRAS, 199, 883-903
- Bolton, J.G. & Stanley, G.J. 1948, Australian Journal of Scientific Research, 1, 57-69
- Bower, G.A. et al. 2000, ApJ, 534, 189-200
- Boyle, B.J. et al. 2000, MNRAS, 317, 1014-1022
- Burke, B.F. & Graham-Smith, F. 2010, *Radio Astronomy*, 3rd Edition, 13: 287-316, CUP, UK
- Byrd, G.G. et al. 1987, A&A, 171, 16-24
- Camenzind, M. 2002, *Quasars and Rotating Black Holes* website
http://www.lsw.uni-heidelberg.de/users/mcamenzi/Quasars_1.pdf (accessed 17 Sept. 2011)
- Cisternas, M. et al. 2011, ApJ, 726, article id. 57
- Curtis, H.D. 1918, Publications of the Lick Observatory, 13,31
- Eisenhauer, F. 2008, ApJ, 628, 246-259
- Emerson, D. 1996, *Interpreting Astronomical Spectra*, John Wiley & Sons, New York, 255
- Falcke, H. 2008, *Physics of Active Galactic Nuclei and Black Holes* website
<http://www.astro.ru.nl/~falcke/AGN/> (accessed 17 Sept. 2011)
- Fan, X. 2003, AJ, 125, 1649-1659
- Fath, E.A. 1908, Lick Observatory Bulletin, 19, 33
- Ferrarese, L. & Merritt, D. 2000, ApJ, 539, L9-L12
- Fitzpatrick, R. 2002, *Electromagnetic Wave Propagation in Dielectrics* website
<http://farside.ph.utexas.edu/teaching/jk1/lectures/node85.html> (accessed 9 Nov. 2011)
- Flynn, C. 2005, *Astrophysics II: Radiation Processes in Astrophysics* website
<http://www.astro.utu.fi/~cflynn/astroll/> (accessed 9 Nov. 2011)
- Franceschini, A. et al. 1999, MNRAS, 310, L5-L9
- Frank, J. et al. 2002, *Accretion Power in Astrophysics*, 3rd Edition, 230
- Gallimore et al. 2010, *Cold Gas Near Active Galactic Nuclei*
<http://www.eg.bucknell.edu/physics/gallimore/gallimore.pdf> (accessed 12 Nov 2011)
- Gebhardt, K. et al. 2000, ApJ, 539, L13-L16
- Ghez, A.M. 1998, ApJ, 509, 678-686
- Ghez, A.M. et al. 2008, ApJ, 689, 1044
- Ghosh, P. & Abramowicz, M.A. 1997, MNRAS, 292, 887-895
- Gillessen, S. et al. 2009, ApJ, 692, 1075-1109
- Gray, R.O. & Corbally, C.J. 2009, *Stellar Spectral Classification*, Princeton Univ. Press, 550
- Greenstein, J. L. & Matthews, T.A. 1963, AJ, 68, 20
- Gunn, J.E. 1979, in Hazard, C. & Mitten, S. (eds), *Active Galactic Nuclei*, CUP, 213
- Hawkins, R.M.S. 2004, A&A, 424, 519-529
- Heckman, T.M. 1980, A&A, 87, 152-164
- Hernquist, L. 1989, Nature, 340, 687-691
- Hey, J.S. et al. 1946, Nature, 158, 234
- Hoffmeister, C. 1929, Astronomische Nachrichten, 236, 233
- Hunt, L.K. & Malkan, M.A. 2004, ApJ, 616, 707-729
- Jennison, R.C. & Das Gupta, M.K. 1953, Nature, 172, 996-997
- Jones, M.H. & Lambourne, R.J.A (eds). 2003, *An Introduction to Galaxies and Cosmology*, CUP, UK, 2:99; 3:123-168,
- Kaufmann III, W.J. 1979, *Galaxies and Quasars*, W.H. Freeman & Co.
- Khachikian, E.E. & Weedman, D.W. 1974, ApJ, 192, 581-589
- Koide, S. 2004, ApJ, 606, L45-L48
- Kormendy, J. & Richstone, D. 1995, ARA&A, 33, 581-624
- Kutner, M. L. 2003, *Astronomy, A Physical Perspective*, CUP, 8:148-149; 19:353-375
- Lynden-Bell, D. 1969, Nature, 223, 690-694
- Maciejewski, W. 2004, Proceedings IAU Symposium, 222, 431-434

Magorrian, J. et al. 1998, AJ, 115, 2285-2305
Martini, P. 2004, Proceedings IAU Symposium, 222, 235-241
Matthews, T.A. & Sandage, A.R. 1963, ApJ, 138, 30-58
Merritt, D. & Ferrarese, L. 2001, MNRAS, 320, L30-L34
Merritt, D. et al. 2001, Science, 293, 1116-1118
Migliori, G. 2010, *High Energy Emission in Relativistic Jets of AGN*, Ph. D Thesis
Scuola Internazionale Superiore di Studi Avanzati
Minkowski, R. 1960, ApJ, 132, 908-910
Miyaji, T. et al. 2001, A&A, 369, 49-56
Miyoshi, M et al. 1995, Nature, 373, 127-129
Moran, J. et al. 1995, Proc. National Academy of Sciences USA, 92, 11427-11433
Narayan, R. & Quataert, E. 2005, Science, 307, 77-80
Oke, J.B. et al. 1969, ApJ, 156, L41-L43
Oke, J.B. & Gunn, J.E. 1974, ApJ, 189, L5-L8
Osterbrock, D.E. et al. 1976, ApJ, 206, 898-909
Osterbrock, D.E. 1977, ApJ, 215, 733-745
Osterbrock, D.E. 1978, Physica Scripta, 17, 137-143
Osterbrock, D.E. & Ferland, G.J. 2006, *The Astrophysics of Gaseous Nebula and Active Galactic Nuclei*, University Science Books, Sausalito, CA, 13:325-351
Ostlie, D.A. & Carroll, B.W. 2007, Introduction to Stellar Astrophysics, Pearson Addison Wesley, 69
Padovani, P. & Urry, C.M. 1991, ApJ, 368, 373-379
Page, M.J. et al. 1997, MNRAS, 291, 324-336
Pearson, T.J. et al. 1981, Nature, 290, 365-368
Perley, R.A. et al. 1984, ApJ, 285, L35-L38
Peterson, B.M. 1997, *Active Galactic Nuclei*, CUP, UK, 1:1-20; 2:21-31
Peterson, B.M. et al. 2004, ApJ, 613, 682-689
Peterson, B.M. & Wilkes, B. J. 2006, in Murdin, P. (ed), *Encyclopedia of Astronomy*, IOP Publishing
Piner, B.G. et al. 2003, ApJ, 588, 716-730
Pogge, R.W. & Martini, P. 2002, ApJ, 569, 624-640
Prieto, M.A. et al. 2005, AJ, 130, 1472-1481
Rees, M.J. 1966, Nature, 211, 468-470
Roy, A. et al. 1994, ApJ, 432, 496-507
Salpeter, E.E. 1964, ApJ, 140, 796-800
Schilling, G. 2011, *Atlas of Astronomical Discoveries*, Springer, 143
Schmidt, M. 1963, Nature, 197, 1040
Schmitt, J.L. 1968, Nature, 218, 663
Schödel, R. et al. 2002, Nature, 419, 694-696
Schwarz, M. 1981, ApJ, 247, 77-88
Semakin, N.K. 1955, Variable Stars (Moscow), 10, 283
Semenov, V. et al. 2004, Science, 305, 978-980
Seyfert, C. K. 1943, ApJ, 97, 28-40
Shankar, F. 2009, New Astronomy Reviews, 53, 57-77
Shlosman, I. (ed) 1994, *Mass-Transfer Induced Activity in Galaxies*, CUP
Slipher, V.M. 1917, Lowell Observatory Bulletin, 80, 59-62
Sparke, L.S. & Gallagher, J.S. 2007, Galaxies in the Universe, CUP, 1:46; 9:365-389
Steinicke, W. Cygus A: *Observing an Exceptional Radio Galaxy* website
http://www.klima-luft.de/steinicke/Artikel/cyga/cyga_e.htm (accessed 4 Nov. 2011)
Stone, J.M. et al. 1996, ApJ, 463, 656-673
Strittmatter, P.A. et al. 1972, ApJ, 175, L7-L13
Toomre, A. & Toomre, J. 1972, ApJ, 178, 623-666
Tour of the Radio Universe website
<http://www.cv.nrao.edu/course/astr534/Tour.html> (accessed 4 Nov. 2011)
Urry, C.M. & Padovani, P. 1995, PASP, 107, 803-845
Whittle, M. 2011, *Extragalactic Astronomy I and II* website
<http://www.astro.virginia.edu/class/whittle/astr553/Syllabus.html> (accessed 6 Nov. 2011)
Woo, J-H. & Urry, C. M. 2002, ApJ, 581, L5-L7
York, D. et al. 2000, AJ, 120, 1579-1587